Probing DNA melting behaviour under vibrational strong coupling

Weijian Tao[1], Fatma Mihoubi[1,2], Bianca Patrahau[1], Claudia Bonfio[1,2], Bengt Nordén[3] and Thomas W. Ebbesen[*1]

[1] University of Strasbourg and CNRS, ISIS & icFRC, Strasbourg, France

[2]University of Cambridge, Department of Biochemistry, Cambridge, UK

[3]Chalmers University of Technology, Department of Chemical and Biological Engineering, Gothenburg, Sweden

Manipulating matter by strong coupling to the vacuum field has attracted intensive interests over the last decade. In particular, vibrational strong coupling (VSC) has shown great potential for modifying ground state properties in solution chemistry and biochemical processes. In this work, the effect of vibrational strong coupling (VSC) of water on the melting behaviour of ds-DNA, an important biophysical process, is explored. Several experimental conditions, including the concentration of ds-DNA, cavity profile, solution environment, as well as thermal annealing treatment were tested. No significant effect of VSC was observed for the melting behaviour of the ds-DNA sequence used. This demonstrates yet again the robustness of ds-DNA to outside perturbations. Our work also provides a general protocol to probe the effects of VSC on biological systems inside microfluid Fabry-Perot cavities and should be beneficial to better understand and harness this phenomenon.

This peer-reviewed article has been accepted for publication but not yet copyedited or typeset, and so may be subject to change during the production process. The article is considered published and may be cited using its DOI.

10.1017/qrd.2025.5

Keywords: light-matter interaction; vibrational strong coupling; DNA; melting behaviour.

Introduction

The last decade has witnessed a fast-growing interest in manipulating matter by strong coupling to the so-called vacuum electromagnetic field (Garcia-Vidal et al. 2021; Nagarajan et al. 2021). For instance, strong coupling between electronic transitions of molecules and optical modes has shown great potential for modifying photochemistry (Hutchison et al. 2012; Zeng et al. 2023), energy transport (Zhong et al. 2016; Zhong et al. 2017; Sandik et al. 2024) and charge carrier conductivity (Orgiu et al. 2015; Nagarajan et al. 2020). On the other hand, strong coupling between vibrational transitions of molecules and the vacuum field, known as vibrational strong coupling (VSC), has also shown great potential for modifying ground-state processes, such as chemical reactivity (Thomas et al. 2016; Thomas et al. 2019; Pang et al. 2020; Nagarajan et al. 2021; Ahn et al. 2023; Patrahau et al. 2024), supramolecular assemblies (Hirai et al. 2021; Joseph et al. 2021; Sandeep et al. 2022; Joseph et al. 2024) and electrochemistry (Fukushima et al. 2022; 2023). The strong coupling conditions are usually achieved by collective coupling of a large number (N) of molecules with an optical mode of a Fabry-Perot cavity, which gives rise to two hybrid polaritonic states (upper and lower polaritonic states, UP and LP respectively) and N-1 dark collective states (DS). It is important to note that strong coupling occurs even in the dark due to involvement of the electromagnetic fluctuations of the cavity (i.e. the vacuum field). VSC can be achieved either by coupling directly to the cavity a vibration of the target molecule or indirectly by the so-called cooperative coupling where solvent and solute vibrations are coupled simultaneously to the same cavity mode (Lather et al. 2019; Schütz et al. 2020).

In biology, VSC has also been harnessed to modify biochemical processes such as enzymatic activity in aqueous solution (Vergauwe et al. 2019; Lather and

https://doi.org/10.1017/qrd.2025.5 Published online by Cambridge University Press

George 2021; Gao et al. 2023; Gu et al. 2023). The ubiquity of water as the natural medium for biological activities makes it the optimal solvent for exploring biochemical processes. Furthermore, VSC of water is typically in the ultra-strong regime (where the energy separation of UP and LP is larger than 10% of the vibrational band) (Fukushima et al. 2021; Kadyan et al. 2024) and can be even observed in micro-sized water droplets without photonic structures (Canales et al. 2024). Thus, water is an excellent solvent to explore VSC induced effects in biochemical and biophysical processes.

Double-stranded deoxyribonucleic acid (dsDNA) is a key supramolecular structure in biological systems, comprising two sequence-complementary DNA strands held together in a double-helix by non-covalent interactions, e.g. hydrogen bonding between nucleotide base pairs. The non-covalent interactions provide dsDNA high thermodynamic stability in biological environments, which is crucial for their functionalities allowing DNAs to interact with a range of biological molecules, (Norden and Kurucsev 1994; Jensen et al. 1997; Vologodskii and Frank-Kamenetskii 2018). The stability of dsDNA helixes depends among other things on the composition and sequence of the individual DNA strands, which in turn determine the strength of several non-covalent interactions, such as hydrogen bonding, dipole-dipole, dipole-induced dipole and London dispersion forces (Devoe and Tinoco 1962; Yakovchuk et al. 2006; Vologodskii and Frank-Kamenetskii 2018; Feng et al. 2019; Nordén 2019). The stability of dsDNA also depends on its solvation in solution, thus sensitive to the latter's composition, salt concentration and pH (Vologodskii and Frank-Kamenetskii 2018). The thermodynamic stability of dsDNA can be inferred from their melting behavior, i.e. the dissociation process of dsDNA into single-stranded (ss) DNA. As VSC has been shown to influence non-covalent interactions in chemical and biological systems (Joseph et al. 2021; Sandeep et al. 2022; Joseph et al. 2024; Patrahau et al. 2024), we sought to explore how VSC influences the stability of dsDNA. Notably, it was recently reported that VSC

https://doi.org/10.1017/qrd.2025.5 Published online by Cambridge University Press

affects the hybridization process of DNA, with the thermal stability of the resulting DNA was analyzed outside the optical cavity after VSC (Hou et al. 2024).

Probing dsDNA melting inside a Fabry-Perot cavity (an optical cavity consisting of two parallel mirrors) using common spectroscopy techniques remains a significant challenge due to several issues, including the limited optical pathlengths of the infrared (IR) cavities (~10 μm), the low transmission in the UV-visible region due to the metallic mirrors (less than 10%) and the low sample concentrations usually used for biological samples (1-10 μM). Therefore, employing fluorescence spectroscopy represents a promising approach, thanks to its high sensitivity. In addition, fluorescence spectroscopy based on Förster resonance energy transfer (FRET) is widely used to study biological processes (Ha 2001; Quan et al. 2020), including the denaturation of nucleic acids (Johansson et al. 2002; Marras et al. 2002).

In this work, we used our newly developed microfluid cavities (Patrahau et al. 2024) as a platform to probe the effects of VSC on the melting behavior of dsDNA under equilibrium condition. These microfluid cavities made in fused silica substrates support multiple cavity modes in the IR region and allow for sufficient light outcoupling in the UV-visible region for luminescence measurements. Additionally, they offer several advantages such as fixed and homogeneous pathlength everywhere in the cavity with good thermal stability against temperature variations. A set of Fabry-Perot cavities with different pathlengths allows us to choose the right one for coupling the vibrational modes of water and thereby study systematically the effects induced by VSC.

Methods

Sample preparation

https://doi.org/10.1017/qrd.2025.5 Published online by Cambridge University Press

The DNA oligonucleotides used in this work were purchased from Integrated DNA Technologies (IDT) with HPLC purification. The sequences used for all experiments were as follows:

Strand 1: 5'-FAM-ACTCGCACCTAGT-3'

Strand 2: 5'-ACTAGGTGCGAGT-BHQ1-3'

where FAM and BHQ1 on strand 1 and strand 2 are, respectively, a fluorescein emitting moiety and a so-called black hole quencher. FAM was chosen as a fluorescence reporter for its high extinction coefficient (~76900 $M^{-1}\cdot cm^{-1}$) and its near-unity fluorescence quantum yield (~0.93) (Sjöback et al. 1995). BHQ-1 is a widely used quencher for FAM.

Oligonucleotides were rehydrated in Milli-Q water to a final concentration of ~500 μM. Concentrations were confirmed by UV absorbance at 260 nm using the extinction coefficients provided by IDT (141,560 M^{-1} cm^{-1} for strand 1 and 138,700 M^{-1} cm^{-1} for strand 2). A stock solution of dsDNA was prepared by mixing equimolar amounts of strand 1 and strand 2 solution in a 10 mM sodium phosphate buffer (pH 7.0) in a final concentration of 10 μM. The mixture was heated between 65 and 75 °C, i.e., above the melting temperature estimated for the dsDNA system ($T_m \approx$ 50 °C), for 15 minutes using a heating block (Thermo Fisher Scientific, Inc.). The solution was then allowed to slowly cool down to room temperature to ensure the assembly of dsDNA. Samples were either used immediately or stored at −4 °C.

To prepare 1 μM dsDNA solution samples, the 10 μM dsDNA stock solution was further diluted 10 times in 10 mM sodium phosphate buffer (pH 7.0). For dsDNA samples in D_2O/H_2O (90%/10%) mixed solvent, the stock solution was diluted with D_2O.

Fabry-Perot microfluid cavities

The microfluid cavities were fabricated by LioniX International and consist of fused silica substrates coated with 10 nm gold (Au) mirrors. An additional SiO_x

https://doi.org/10.1017/qrd.2025.5 Published online by Cambridge University Press

layer (100 nm) was coated to protect the Au mirrors and to prevent any potential fluorescence quenching by physical contact with the gold. Reference structures without Au mirrors were also prepared. Schematic illustrations of the microfluid cavities and the reference structures are shown in Fig. S1. More detailed descriptions about the microfluid cavities can be found in previously published work (Patrahau et al. 2024).

Melting curve measurements

dsDNA solutions were gently injected into microfluid cavities with a syringe equipped with a flat needle. The cavity was sealed at each end with round glass platelets (Φ= 3 mm) and thin tape. Glue or wax as sealant was avoided not to contaminate the samples. The dsDNA melting curve measurements inside microfluid cavities were performed in a home-built high-sensitivity fluorescence setup (Fig. S2). To perform temperature-dependent measurements, the cavities were fixed onto a commercial temperature-controlled sample holder (CD 250, Quantum Northwest, Inc., equipped with a temperature controller TC1, Quantum Northwest, Inc.). An electronic controlled optical beam shutter (SH1 and SC10, Thorlabs Inc.) was employed to minimize photobleaching and only allow laser illumination during the fluorescence measurements. Optical filters (Semrock, Inc.) optimized for the FAM fluorophore were used for collecting the signal and attenuating the excitation beam. Note that the shape of the FAM fluorescence spectrum (Fig. 1b) is modified by the use of a dichroic beam-splitter with an edge at 506 nm, and 540/50 nm bandpass for collection. The cutoff close to 570 nm is due to this bandpass filter.

To ensure thermal equilibrium at each temperature, cavities were held at the set temperature for 5 minutes before recording the emission spectrum, except when testing temperature ramping effects. By plotting the maximum emission intensity of the collected spectra as a function of temperature (Fig. 1b), melting

https://doi.org/10.1017/qrd.2025.5 Published online by Cambridge University Press

curves as shown in Fig. 1c were obtained. Measurements were repeated several times for each experimental condition to ensure reproducibility. It should be noted that the FAM emission intensity is by itself insensitive to VSC of water. It does show a small temperature variation of about 10% (Fig. S3).

Figure 1 should be here

Figure 1. Principle and protocol for probing melting behaviour of ds-DNA inside microfluidic cavity. (a) schematic illustration of the principle of measurement based on FRET process (yellow cavity field, green melting curve as a function of temperature). (b) measured fluorescence spectra at different temperatures of ds-DNA at 1 μM in the reference structure (R0) (c) extracted melting curves from four independent measurements in R0, with their corresponding first derivatives shown in (d).

Results

To begin we established a general experimental protocol, by measuring melting curves of dsDNA inside the reference structure R0. In the latter, the microfluidic channel is without mirrors and the two substrates are spaced by 12 μm. R0 thus acts as a control in our experiments. Fig. 1a demonstrates the principle of our measurements of melting curves based on the FRET mechanism. The fluorescein (FAM) and the black hole quencher (BHQ-1) (described in the Methods section) form a FRET pair. When the two fluorophores are in proximity, as in the case of the dsDNA involved in this study, the FAM fluorescence is quenched by BHQ-

https://doi.org/10.1017/qrd.2025.5 Published online by Cambridge University Press

1. At high temperatures, dsDNA disassembles into two ssDNA oligonucleotides, and the fluorescence of FAM is restored.

A 1 uM dsDNA solution was injected into the reference structure R0, which was fixed onto a temperature-controlled sample holder, then cooled down to 12 °C and held for an additional 1 hour before measurements, thereby ensuring that all DNA is in a double-stranded state. Even then some residual background emission can be detected with the high sensitivity of the setup. Therefore, this background spectrum collected at 12 °C was subtracted from all the spectra collected at higher temperatures. Fig. 1b shows an example of fluorescence spectra measured in R0 where the intensity increases monotonously with temperature. The emission intensities were further averaged over a large spectral range (from 510 nm to 550 nm), yielding the melting curves shown in Fig. 1c. The intensity reaches a plateau at ca. 55°C, suggesting that dsDNA is dissociated into ssDNA above this temperature. As shown in Fig. 1c, the melting curves extracted from four independent measurements are superimposable, demonstrating a high reproducibility of our protocol. The melting temperature is defined as the temperature at which half of dsDNA are dissociated into ss-DNA. To quantitively extract the melting temperature and its standard deviation, a first-derivative analysis was performed (Owczarzy 2005). As shown in Fig. 1d, the analysis yields a melting temperature of 46.5 ± 1.0 °C for the ds-DNA for the non-optical cavity conditions of reference R0.

Figure 2 should be here

Figure 2. Melting behaviour of ds-DNA at 1 μM inside microfluid cavities. (a) FTIR spectra of cavity S1 filled with ds-DNA solution, also shown in black line is the IR band of OH stretching mode of water. The cavity mode position is indicated in grey dashed line. (b) The melting curves of ds-DNA in cavity S1 and reference structure R0.

https://doi.org/10.1017/qrd.2025.5 Published online by Cambridge University Press

We then performed similar measurements with cavity S1, which has the same depth as reference structure R0, i.e. 12 μm. The presence of the two gold mirrors in cavity S1 gives rise to multiple well-defined cavity modes in the infrared (IR) region, as shown in Fig. S3. The free spectral range (FSR) of cavity S1 is measured to be 415 cm^{-1} and full width of half-maximum (FWHM) of 64 cm^{-1}, resulting in a cavity quality factor Q of 52. The eight-cavity mode at 3320 cm^{-1} indicated by the grey dashed line in Fig.2a has a good overlap with the broad OH stretching band of water at 3300 cm^{-1} measured by attenuated total reflection (ATR) (black line in Fig. 2a). After injecting the solution, two polaritonic bands emerge around the spectral region of the OH stretching band (green line in Fig. 2a), with LP band at 2922 cm^{-1} and UP band at 3683 cm^{-1}, The Rabi splitting is estimated to be ~ 762 cm^{-1}. The Rabi splitting is much larger than either the FWHM of the OH stretching band (445 cm^{-1}) and the FWHM of the cavity mode (64 cm^{-1}), indicating that the system under investigation entered collective VSC.

The average melting curve of dsDNA inside cavity S1 is shown in Fig. 2b, together with that obtained with the reference structure R0. As shown, no significant difference was observed between the melting curves of dsDNA inside cavity S1 and that in R0. The first-derivate analysis gives a melting temperature of 47.0 ± 0.0 ℃ for the dsDNAs inside cavity S1, which is within experimental error the same as inside the reference structure R0 (46.5 ± 1.0 ℃).

To explore if cavity detuning influences the effects of VSC on the studied system, we further performed melting curve measurements (Fig. S4) and the first derivative analysis (Fig. S5) with other cavities of different FSRs and cavity profiles (cavity S2-S4, shown in Table 1). However, no significant change of melting temperatures was observed across different cavity detuning, as shown in Table 1, and illustrated in Fig. S6.

Table 1 Melting temperatures of ds-DNA under various experimental conditions and determined by first-derivative analysis

https://doi.org/10.1017/qrd.2025.5 Published online by Cambridge University Press

Table 1 should be here

Besides the base composition and sequence of dsDNA, the melting behavior of dsDNA is also known to depend on the DNA concentration and solution composition (Vologodskii and Frank-Kamenetskii 2018). Furthermore, recent work demonstrated that the effects of VSC on supramolecular polymerization of porphyrins are highly dependent on concentration and solvent (Joseph et al. 2024). The modification of ionic conductivity in aqueous solution through VSC was also shown to be sensitive to the composition of the electrolytes (Fukushima et al. 2023). Therefore, we further extended our measurements to a concentration ten times higher (10 μM) and also explored the effect of D_2O. As shown Table 1, the melting temperature increases at higher dsDNA concentrations as expected (Breslauer 1994; Vologodskii and Frank-Kamenetskii 2018). Still, no change was observed under VSC. The corresponding melting curves of dsDNA at 10 μM inside the reference structure R0 and two representative cavities S1 and S4 are shown in Fig. S7.

Figure 3 should be here

Figure 3. Melting behaviour of ds-DNA under other conditions. (a) FTIR spectrum of D_2O/H_2O (90%/10%) solution. (b) the melting curves of ds-DNA in reference structure R0 and cavity S1. (c) the melting curve after annealing in reference structure R0 and cavity S1. Also shown is the melting curve of ds-DNA without annealing in cavity S1.

We further prepared a 1 μM dsDNA solution in D_2O/H_2O (90%/10%) mixed solvent. D_2O has stronger hydrogen bonding than H_2O, thus different solvent properties (Giubertoni et al. 2023). The FTIR spectra of D_2O/H_2O (90%/10%) solution in reference structure R0 and cavity S1 are shown in Fig. 3a. In reference structure R0, the vibrational bands of OH stretching and OD stretching were clearly observed at 3411 cm^{-1} and around 2500 cm^{-1}, respectively. In cavity S1, several polaritonic modes were observed due to the coupling between different

https://doi.org/10.1017/qrd.2025.5 Published online by Cambridge University Press

cavity modes and solvent IR bands. The melting curves of dsDNA in the mixed D_2O/H_2O solution shifted to a lower temperature, compared with the melting curves measured in pure H_2O solution (Fig. 2b), as expected (Hou et al. 2024). Once again, no significant difference was observed under VSC (Fig. 3b).

During the measurement of the melting curves in D_2O/H_2O solution, we noticed that the proton exchange process between H_2O and D_2O is very slow (hour timescale) (Printz and Vonhippel 1965). As proposed in a theoretical study, the hydration spine present in the minor groove of dsDNA is frozen in the helix and behaves as an integral part of double helix, which increases the thermal stability of dsDNA (Chen and Prohofsky 1993). The slow proton exchange indeed influenced the melting behavior of fresh and aged samples (Fig. S8).

To ensure that such slow feature did not affect other experiments, we repeated the study of the melting curves in H_2O first annealing the samples under VSC. The dsDNA solution inside microfluid cavities was heated up to 75 °C and annealed for 1 hour to fully dissociate the DNA into single stranded state and to fully exchange the proton between the water inside the minor grooves of dsDNA and the solution. Then the cavities were slowly cooled down to 12 °C and kept at that temperature for 1 hour, during which time the ssDNA re-hybridized into dsDNA again, but under VSC. Again, this protocol didn't introduce any difference on the melting temperatures of ds-DNA (Fig. 3c) whether measured in the reference structure R0 or in the cavity S1.

Discussion

In summary, no significant effect from VSC on the melting curves dsDNA was found for all tested conditions, which included cavity detuning, DNA concentration and solvent composition. One key difference between our work and the previous study (Hou et al. 2024) is that the melting behavior was measured in equilibrium condition in our case, while in the previous work by Hou et al. it was measured in a continuous manner at a rapid ramp rate (2°C/min).

https://doi.org/10.1017/qrd.2025.5 Published online by Cambridge University Press

Therefore, we repeated our experiments at a similar ramp rate and without equilibrating the DNA at each temperature, but again no significant difference was observed (Fig. S9), which further rules out the possibility of a kinetic effect from VSC in our system.

In fact, our experiments are fundamentally different from the earlier work on DNA under VSC by Hou el.al (2024). In that work, the ssDNA solution was first injected into the optical cavity and the formation of dsDNA was performed in situ at room temperature. The melting curves were then determined outside the cavity by fluorescence measurements and a decrease in Tm was found under VSC. This protocol assumes that the effects of VSC remain after extraction from the cavity. This would imply a stable structural change under VSC which we do not detect with our DNA strand composition. In other words, it is possible that the difference in the results stems from the nucleotide composition differences in the two studies.

The insensitivity of the thermal stability of dsDNA to VSC is in strong contrast to the supramolecular polymerization of porphyrins, where even the relative stability between monomer and polymer can be reversibly tuned by VSC (Joseph et al. 2024). The sensitivity of these porphyrin assemblies to VSC is probably due to the dynamic monomer addition and dissociation in solution and the related pathway complexity, which makes the system very sensitive to external stimuli (Mabesoone et al. 2018).

The fact that we detect no effect of VSC on the melting behavior of DNA cannot be due to lack of cooperative coupling between the stretching mode of H_2O and the vibrational modes of DNA. The vibrational frequency of OH stretching mode of H_2O at around 3300 cm^{-1} is well-known to be very sensitive to the strength of hydrogen bonding (Brubach et al. 2005). For liquid water, there are at least three Gaussian components within the spectral profile of the OH stretching mode at 3295 cm^{-1}, 3460 cm^{-1} and 3590 cm^{-1}, which correspond to subpopulations of water clusters (Brubach et al. 2005). The vibrational frequency

https://doi.org/10.1017/qrd.2025.5 Published online by Cambridge University Press

of NH stretching mode in DNA pairs also lies between 3300 cm^{-1} to 3600 cm^{-1} (Nir et al. 2002), having good overlap with the OH stretching mode of water. Therefore, the reason for the results must be other than an issue of cooperativity, reflecting the nature of the interaction forces at play in the DNA structure.

The thermal stability of dsDNA is mainly determined by base-stacking interactions which are partially from London dispersion forces and partially from hydrophobic interactions, and less by base pairing interactions, i.e. hydrogen bonding (Herskovits 1962; Yakovchuk et al. 2006; Vologodskii and Frank-Kamenetskii 2018; Feng et al. 2019; Nordén 2019). In our experiments, the water OH stretching mode is coupled to the vacuum field, where the hydrogen bonds between base pairs are also cooperatively coupled. The less important role of hydrogen bonding on thermal stability of ds-DNA is consistent with the absence of a VSC effect. Furthermore, these hydrogen bonds are buried inside the double helix, which might also be the reason why VSC doesn't alter the thermal stability of ds-DNA. Therefore, our observation of stability of dsDNA to VSC can be considered as another new piece of evidence for the robustness of dsDNA.

Supplementary Material

The supplementary material provides additional illustrations of the cavities used, FTIR spectra and various melting curves under different conditions in support of the results reported here.

Author contributions

BN suggested the experiments. FM and CB designed the DNA sequence and prepared the corresponding samples. WT built the emission setup and carried out most of the VSC experiments. BP helped in the initial experiments and TWE supervised the project.

https://doi.org/10.1017/qrd.2025.5 Published online by Cambridge University Press

Financial Support

We acknowledge the support from the International Center for Frontier Research in Chemistry (icFRC, Strasbourg), the Labex NIE Projects (ANR-11-LABX-0058 NIE), CSC (ANR-10-LABX-0026 CSC), USIAS (Grant No. ANR-10-IDEX-0002-02) within the Investissement d'Avenir program ANR-10-IDEX-0002-02 and the ERC (project no 788482 MOLUSC).

Data availability statement

The raw data is available upon reasonable request.

References

Ahn W, Triana JF, Recabal F, Herrera F and Simpkins BS (2023) Modification of ground-state chemical reactivity via light-matter coherence in infrared cavities. *Science* **380**(6650)**,** 1165-1168. https://doi.org/10.1126/science.ade7147.

Breslauer KJ (1994) Extracting Thermodynamic Data From Equilibrium Melting Curves for Oligonucleotide Order-Disorder Transitions. In Agrawal S (ed), *Protocols for Oligonucleotide Conjugates: Synthesis and Analytical Techniques.* Totowa, NJ: Humana Press, 347-372.

Brubach JB, Mermet A, Filabozzi A, Gerschel A and Roy P (2005) Signatures of the hydrogen bonding in the infrared bands of water. *J Chem Phys* **122**(18)**,** 184509. https://doi.org/10.1063/1.1894929.

Canales A, Kotov OV, Kucukoz B and Shegai TO (2024) Self-Hybridized Vibrational-Mie Polaritons in Water Droplets. *Phys Rev Lett* **132**(19)**,** 193804. https://doi.org/10.1103/PhysRevLett.132.193804.

Chen YZ and Prohofsky EW (1993) Synergistic effects in the melting of DNA hydration shell: melting of the minor groove hydration spine in

poly(dA).poly(dT) and its effect on base pair stability. *Biophys J* **64**(5)**,** 1385-1393. https://doi.org/10.1016/S0006-3495(93)81504-2.

Devoe H and Tinoco I, Jr. (1962) The stability of helical polynucleotides: base contributions. *J Mol Biol* **4**(6)**,** 500-517. https://doi.org/10.1016/s0022-2836(62)80105-3.

Feng B, Sosa RP, Martensson AKF, Jiang K, Tong A, Dorfman KD, Takahashi M, Lincoln P, Bustamante CJ, Westerlund F and Norden B (2019) Hydrophobic catalysis and a potential biological role of DNA unstacking induced by environment effects. *Proc Natl Acad Sci U S A* **116**(35)**,** 17169-17174. https://doi.org/10.1073/pnas.1909122116.

Fukushima T, Yoshimitsu S and Murakoshi K (2021) Vibrational Coupling of Water from Weak to Ultrastrong Coupling Regime via Cavity Mode Tuning. *Journal of Physical Chemistry C* **125**(46)**,** 25832-25840. https://doi.org/10.1021/acs.jpcc.1c07686.

Fukushima T, Yoshimitsu S and Murakoshi K (2022) Inherent Promotion of Ionic Conductivity via Collective Vibrational Strong Coupling of Water with the Vacuum Electromagnetic Field. *J Am Chem Soc* **144**(27)**,** 12177-12183. https://doi.org/10.1021/jacs.2c02991.

Fukushima T, Yoshimitsu S and Murakoshi K (2023) Unlimiting ionic conduction: manipulating hydration dynamics through vibrational strong coupling of water. *Chem Sci* **14**(41)**,** 11441-11446. https://doi.org/10.1039/d3sc03364c.

Gao F, Guo J, Si Q, Wang L, Zhang F and Yang F (2023) Modification of ATP hydrolysis by Strong Coupling with O−H Stretching Vibration. *ChemPhotoChem* **7**(4). https://doi.org/10.1002/cptc.202200330.

Garcia-Vidal FJ, Ciuti C and Ebbesen TW (2021) Manipulating matter by strong coupling to vacuum fields. *Science* **373**(6551)**,** eabd0336. https://doi.org/10.1126/science.abd0336.

Giubertoni G, Bonn M and Woutersen S (2023) D_2O as an imperfect replacement for H_2O: problem and opportunity for protein research? J. Phys. Chem. B 127, 8086-8094. https://doi.org/10.1021/acs.jpcb.3c04385

Gu KH, Si QK, Li N, Gao F, Wang LP and Zhang F (2023) Regulation of Recombinase Polymerase Amplification by Vibrational Strong Coupling of Water. *ACS Photonics* **10**(5), 1633-1637. https://doi.org/10.1021/acsphotonics.3c00243.

Ha T (2001) Single-molecule fluorescence methods for the study of nucleic acids. *Curr Opin Struct Biol* **11**(3), 287-292. https://doi.org/10.1016/s0959-440x(00)00204-9.

Herskovits TT (1962) Nonaqueous solutions of DNA: Factors determining the stability of the helical configuration in solution. *Archives of Biochemistry and Biophysics* **97**(3), 474-484. https://doi.org/10.1016/0003-9861(62)90110-8.

Hirai K, Ishikawa H, Chervy T, Hutchison JA and Uji IH (2021) Selective crystallization via vibrational strong coupling. *Chem Sci* **12**(36), 11986-11994. https://doi.org/10.1039/d1sc03706d.

Hou SJ, Gao F, Zhong CJ, Li JW, Zhu Z, Wang LP, Zhao ZX and Zhang F (2024) Vibrational Alchemy of DNA: Exploring the Mysteries of Hybridization under Cooperative Strong Coupling with Water. *ACS Photonics* **11**(3), 1303-1310. https://doi.org/10.1021/acsphotonics.3c01824.

Hutchison JA, Schwartz T, Genet C, Devaux E and Ebbesen TW (2012) Modifying chemical landscapes by coupling to vacuum fields. *Angew Chem Int Ed Engl* **51**(7), 1592-1596. https://doi.org/10.1002/anie.201107033.

Jensen KK, Orum H, Nielsen PE and Norden B (1997) Kinetics for hybridization of peptide nucleic acids (PNA) with DNA and RNA studied with the BIAcore technique. *Biochemistry* **36**(16), 5072-5077. https://doi.org/10.1021/bi9627525.

Johansson MK, Fidder H, Dick D and Cook RM (2002) Intramolecular dimers: a new strategy to fluorescence quenching in dual-labeled oligonucleotide probes. *J Am Chem Soc* **124**(24)**,** 6950-6956. https://doi.org/10.1021/ja025678o.

Joseph K, de Waal B, Jansen SAH, van der Tol JJB, Vantomme G and Meijer EW (2024) Consequences of Vibrational Strong Coupling on Supramolecular Polymerization of Porphyrins. *J Am Chem Soc* **146**(17)**,** 12130-12137. https://doi.org/10.1021/jacs.4c02267.

Joseph K, Kushida S, Smarsly E, Ihiawakrim D, Thomas A, Paravicini-Bagliani GL, Nagarajan K, Vergauwe R, Devaux E, Ersen O, Bunz UHF and Ebbesen TW (2021) Supramolecular Assembly of Conjugated Polymers under Vibrational Strong Coupling. *Angew Chem Int Ed Engl* **60**(36)**,** 19665-19670. https://doi.org/10.1002/anie.202105840.

Kadyan A, Suresh MP, Johns B and George J (2024) Understanding the Nature of Vibro-Polaritonic States in Water and Heavy Water. *Chemphyschem* **25**(4)**,** e202300560. https://doi.org/10.1002/cphc.202300560.

Lather J, Bhatt P, Thomas A, Ebbesen TW and George J (2019) Cavity Catalysis by Cooperative Vibrational Strong Coupling of Reactant and Solvent Molecules. *Angew Chem Int Ed Engl* **58**(31)**,** 10635-10638. https://doi.org/10.1002/anie.201905407.

Lather J and George J (2021) Improving Enzyme Catalytic Efficiency by Co-operative Vibrational Strong Coupling of Water. *J Phys Chem Lett* **12**(1)**,** 379-384. https://doi.org/10.1021/acs.jpclett.0c03003.

Mabesoone MFJ, Markvoort AJ, Banno M, Yamaguchi T, Helmich F, Naito Y, Yashima E, Palmans ARA and Meijer EW (2018) Competing Interactions in Hierarchical Porphyrin Self-Assembly Introduce Robustness in Pathway Complexity. *J Am Chem Soc* **140**(25)**,** 7810-7819. https://doi.org/10.1021/jacs.8b02388.

Marras SAE, Kramer FR and Tyagi S (2002) Efficiencies of fluorescence resonance energy transfer and contact-mediated quenching in oligonucleotide probes.

Nucleic Acids Research **30**(21)**,** e122-e122. https://doi.org/10.1093/nar/gnf121 %J Nucleic Acids Research.

Nagarajan K, George J, Thomas A, Devaux E, Chervy T, Azzini S, Joseph K, Jouaiti A, Hosseini MW, Kumar A, Genet C, Bartolo N, Ciuti C and Ebbesen TW (2020) Conductivity and Photoconductivity of a p-Type Organic Semiconductor under Ultrastrong Coupling. *ACS Nano* **14**(8)**,** 10219-10225. https://doi.org/10.1021/acsnano.0c03496.

Nagarajan K, Thomas A and Ebbesen TW (2021) Chemistry under Vibrational Strong Coupling. *J Am Chem Soc* **143**(41)**,** 16877-16889. https://doi.org/10.1021/jacs.1c07420.

Nir E, Plützer C, Kleinermanns K and de Vries M (2002) Properties of isolated DNA bases, base pairs and nucleosides examined by laser spectroscopy. *European Physical Journal D* **20**(3)**,** 317-329. https://doi.org/10.1140/epjd/e2002-00167-2.

Nordén B (2019) Role of Water for Life. *Molecular Frontiers Journal* **03**(01)**,** 3-19. https://doi.org/10.1142/s2529732519400017.

Norden B and Kurucsev T (1994) Analysing DNA complexes by circular and linear dichroism. *J Mol Recognit* **7**(2)**,** 141-155. https://doi.org/10.1002/jmr.300070211.

Orgiu E, George J, Hutchison JA, Devaux E, Dayen JF, Doudin B, Stellacci F, Genet C, Schachenmayer J, Genes C, Pupillo G, Samori P and Ebbesen TW (2015) Conductivity in organic semiconductors hybridized with the vacuum field. *Nat Mater* **14**(11)**,** 1123-1129. https://doi.org/10.1038/nmat4392.

Owczarzy R (2005) Melting temperatures of nucleic acids: discrepancies in analysis. *Biophys Chem* **117**(3)**,** 207-215. https://doi.org/10.1016/j.bpc.2005.05.006.

Pang Y, Thomas A, Nagarajan K, Vergauwe RMA, Joseph K, Patrahau B, Wang K, Genet C and Ebbesen TW (2020) On the Role of Symmetry in Vibrational Strong Coupling: The Case of Charge-Transfer Complexation. *Angew Chem Int Ed Engl* **59**(26)**,** 10436-10440. https://doi.org/10.1002/anie.202002527.

Patrahau B, Piejko M, Mayer RJ, Antheaume C, Sangchai T, Ragazzon G, Jayachandran A, Devaux E, Genet C, Moran J and Ebbesen TW (2024) Direct Observation of Polaritonic Chemistry by Nuclear Magnetic Resonance Spectroscopy. *Angew Chem Int Ed Engl* **63**(23)**,** e202401368. https://doi.org/10.1002/anie.202401368.

Printz MP and Vonhippel PH (1965) Hydrogen Exchange Studies of DNA Structure. *Proc Natl Acad Sci U S A* **53**(2)**,** 363-370. https://doi.org/10.1073/pnas.53.2.363.

Quan K, Yi CP, Yang XH, He XX, Huang J and Wang KM (2020) FRET-based nucleic acid probes: Basic designs and applications in bioimaging. *Trac-Trends in Analytical Chemistry* **124**. https://doi.org/ARTN 11578410.1016/j.trac.2019.115784.

Sandeep K, Joseph K, Gautier J, Nagarajan K, Sujith M, Thomas KG and Ebbesen TW (2022) Manipulating the Self-Assembly of Phenyleneethynylenes under Vibrational Strong Coupling. *J Phys Chem Lett* **13**(5)**,** 1209-1214. https://doi.org/10.1021/acs.jpclett.1c03893.

Sandik G, Feist J, Garcia-Vidal FJ and Schwartz T (2024) Cavity-enhanced energy transport in molecular systems. *Nat Mater*. https://doi.org/10.1038/s41563-024-01962-5.

Schütz S, Schachenmayer J, Hagenmüller D, Brennen GK, Volz T, Sandoghdar V, Ebbesen TW, Genes C and Pupillo G (2020) Ensemble-Induced Strong Light-Matter Coupling of a Single Quantum Emitter. *Physical Review Letters* **124**(11)**,** 113602. https://doi.org/10.1103/PhysRevLett.124.113602.

Sjöback R, Nygren J and Kubista M (1995) Absorption and fluorescence properties of fluorescein. *Spectrochimica Acta Part A: Molecular and Biomolecular Spectroscopy* **51**(6)**,** L7-L21. https://doi.org/10.1016/0584-8539(95)01421-p.

Thomas A, George J, Shalabney A, Dryzhakov M, Varma SJ, Moran J, Chervy T, Zhong X, Devaux E, Genet C, Hutchison JA and Ebbesen TW (2016) Ground-State Chemical Reactivity under Vibrational Coupling to the Vacuum

Electromagnetic Field. *Angew Chem Int Ed Engl* **55**(38)**,** 11462-11466. https://doi.org/10.1002/anie.201605504.

Thomas A, Lethuillier-Karl L, Nagarajan K, Vergauwe RMA, George J, Chervy T, Shalabney A, Devaux E, Genet C, Moran J and Ebbesen TW (2019) Tilting a ground-state reactivity landscape by vibrational strong coupling. *Science* **363**(6427)**,** 615-619. https://doi.org/10.1126/science.aau7742.

Vergauwe RMA, Thomas A, Nagarajan K, Shalabney A, George J, Chervy T, Seidel M, Devaux E, Torbeev V and Ebbesen TW (2019) Modification of Enzyme Activity by Vibrational Strong Coupling of Water. *Angew Chem Int Ed Engl* **58**(43)**,** 15324-15328. https://doi.org/10.1002/anie.201908876.

Vologodskii A and Frank-Kamenetskii MD (2018) DNA melting and energetics of the double helix. *Phys Life Rev* **25,** 1-21. https://doi.org/10.1016/j.plrev.2017.11.012.

Yakovchuk P, Protozanova E and Frank-Kamenetskii MD (2006) Base-stacking and base-pairing contributions into thermal stability of the DNA double helix. *Nucleic Acids Research* **34**(2)**,** 564-574. https://doi.org/10.1093/nar/gkj454 %J Nucleic Acids Research.

Zeng H, Perez-Sanchez JB, Eckdahl CT, Liu P, Chang WJ, Weiss EA, Kalow JA, Yuen-Zhou J and Stern NP (2023) Control of Photoswitching Kinetics with Strong Light-Matter Coupling in a Cavity. *J Am Chem Soc* **145**(36)**,** 19655-19661. https://doi.org/10.1021/jacs.3c04254.

Zhong X, Chervy T, Wang S, George J, Thomas A, Hutchison JA, Devaux E, Genet C and Ebbesen TW (2016) Non-Radiative Energy Transfer Mediated by Hybrid Light-Matter States. *Angew Chem Int Ed Engl* **55**(21)**,** 6202-6206. https://doi.org/10.1002/anie.201600428.

Zhong X, Chervy T, Zhang L, Thomas A, George J, Genet C, Hutchison JA and Ebbesen TW (2017) Energy Transfer between Spatially Separated Entangled Molecules. *Angew Chem Int Ed Engl* **56**(31)**,** 9034-9038. https://doi.org/10.1002/anie.201703539.

Table 1 Melting temperatures of ds-DNA under various experimental conditions and determined by first-derivative analysis

Microfluid Cavity	Length (μm)	FSR (cm^{-1})	ds-DNA Concentration (μM)	Tm (°C)
R0	12.0	N/A	1	46.5 ± 1.0
S1	12.0	415	1	47.0 ± 0.0
S2	12.5	395	1	47.5 ± 1.0
S3	13.0	380	1	46.3 ± 2.3
S4	6.0	832	1	46.5 ± 1.2
R0	12.0	N/A	10	50.5 ± 2.1
S1	12.0	415	10	50.0 ± 1.7
S4	6.0	832	10	51.0 ± 1.7

https://doi.org/10.1017/qrd.2025.5 Published online by Cambridge University Press

Figure 1

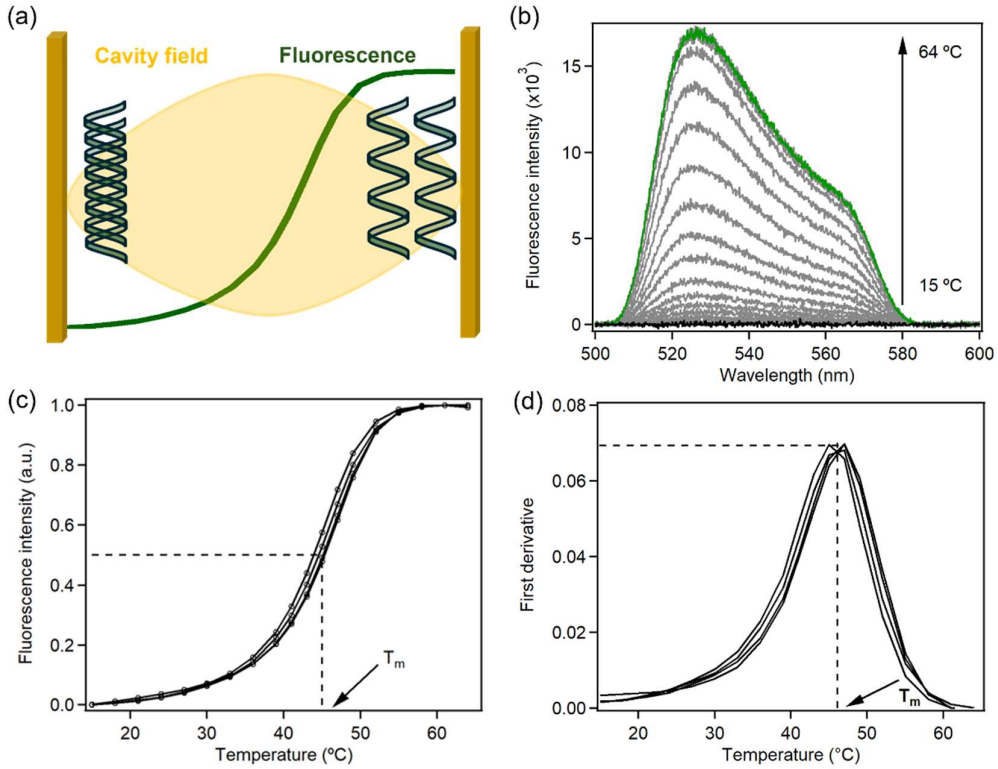

https://doi.org/10.1017/qrd.2025.5 Published online by Cambridge University Press

Figure 2

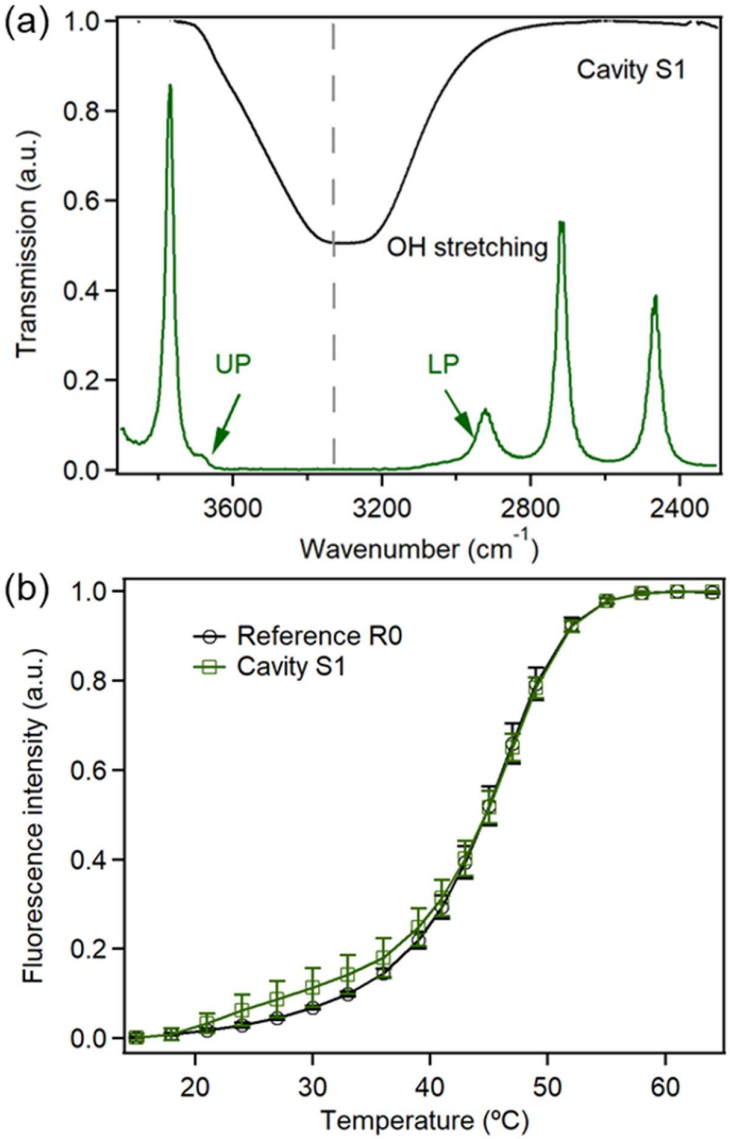

https://doi.org/10.1017/qrd.2025.5 Published online by Cambridge University Press

Figure 3

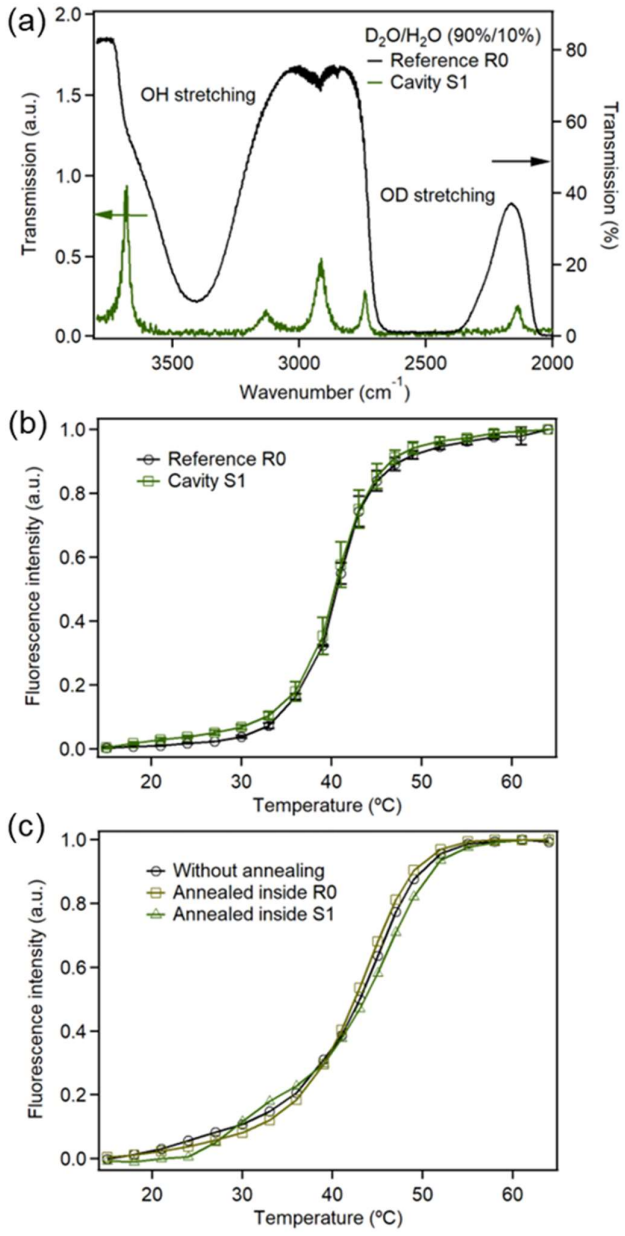

https://doi.org/10.1017/qrd.2025.5 Published online by Cambridge University Press